

A SPARSE GRAPH FORMULATION FOR EFFICIENT SPECTRAL IMAGE SEGMENTATION

Rahul Palnitkar and Jeova Farias Sales Rocha Neto

Haverford College
Department of Computer Science
370 Lancaster Avenue
Haverford, PA 19041

ABSTRACT

Spectral Clustering is one of the most traditional methods to solve segmentation problems. Based on Normalized Cuts, it aims at partitioning an image using an objective function defined by a graph. Despite their mathematical attractiveness, spectral approaches are traditionally neglected by the scientific community due to their practical issues and underperformance. In this paper, we adopt a sparse graph formulation based on the inclusion of extra nodes to a simple grid graph. While the grid encodes the pixel spatial disposition, the extra nodes account for the pixel color data. Applying the original Normalized Cuts algorithm to this graph leads to a simple and scalable method for spectral image segmentation, with an interpretable solution. Our experiments also demonstrate that our proposed methodology over performs traditional spectral algorithms for segmentation.

Index Terms— Image Segmentation, Spectral Clustering, Sparse Matrices, Optimization.

1. INTRODUCTION

Image Segmentation refers to the problem of grouping image pixels in meaningful regions with the goal of understanding or summarizing the visual content in that image [1]. Because of that, image segmentation has found applications in many domains, such as medical image analysis, autonomous driving, and photo editing to name a few [1]. This intense industrial appeal led to the development of many algorithms, which tackled the problem using variational [2], graphical [3, 4, 5], statistical [6] and, more recently, deep learning techniques [7].

Spectral clustering [8], pioneered by Normalized Cuts [3], provides an algorithm for image segmentation that stands out for its methodological consistency backed by graph theory and computational linear algebra. It consists of encoding the image data into a graph then using spectral techniques to approximately find the cut corresponding to the final segmentation. While popular in its early years, the initial formulation of Normalized Cuts had that would hinder its broad adoption by the scientific community. The issues found were mostly (1) computational, as it required the construction and

decomposition of large matrices [9], and (2) practical, as it performed worse than other algorithms [10].

Many strategies were approached to overcome the issues [9, 11, 12, 13]. In this paper, we approach them by adopting a sparse graph consisting of a grid graph that encodes the pixel spatial locations and of a few extra nodes corresponding to the pixel intensities [2, 4]. We show that the Normalized Cut solution found using this graph encourages pixel groupings that linearly balances spatial coherence (neighbors generally belong to the same segment) and color cohesion (pixels in a segment have colors in the same subset of available colors) [14]. Furthermore, we also demonstrate that our proposed spectral method is scalable and easily tunable, besides being easy to implement. Finally, we compare our method to other traditional spectral techniques for segmentation and observe that it outperforms them in terms of runtime and quality.

The next sections are organized as follows: In Section 2, we show an overview of Normalized Cuts, its main algorithm, and drawbacks. In Section 3, we present our proposed graph construction and characterize the solution of Normalized Cuts when optimized to it. Experimental results are presented in Section 4 along with a brief discussion on them. We finish with conclusions and future work in Section 5.

2. BACKGROUND

2.1. Normalized Cuts

Let I be an image of n pixels and k unique colors. Let $G = (V, E, w)$ be an undirected weighted graph where each node corresponds to a pixel and the weight function $w(i, j)$ evaluates the similarity between pixels i and j . A binary segmentation of I is achieved by finding a partition (A, B) of V that minimizes the cut value $\text{Cut}(A, B) = \sum_{i \in A, j \in B} w(i, j)$.

This approach however favors unbalanced partitions, leading to undesirable segmentations. One successful way of addressing this issue is to consider the *normalized cut* value $\text{NCut}(A, B)$ [3] instead,

$$\text{NCut}(A, B) = \frac{\text{Cut}(A, B)}{\text{Vol}(A)} + \frac{\text{Cut}(A, B)}{\text{Vol}(B)}.$$

Here $\text{Vol}(A)$ is a measure of the ‘‘volume’’ of A defined as $\text{Vol}(A) = \sum_{i \in A, j \in V} w(i, j)$. Later, we use $\text{Vol}(V) = \text{Vol}(A) + \text{Vol}(B)$ to represent the volume of all edges in G .

Let W be the weighted adjacency matrix of G and D be the diagonal degree matrix with $D(i, i) = \sum_{j \in V} w(i, j)$. The Laplacian matrix of G is then defined as $L = D - W$. Following the derivation presented in [15], we can write the problem of minimizing the NCut of G as:

$$\begin{aligned} \min_{\mathbf{x}} \quad & \mathcal{E}(\mathbf{x}|G), \\ \text{s.t.} \quad & \mathbf{x}^\top D \mathbf{x} = 1, \quad \mathbf{1}^\top D \mathbf{x} = 0, \quad \mathbf{x} \in \{-\alpha, \beta\}^n. \end{aligned} \quad (1)$$

where \mathbf{x} is the vector that corresponds to our final segment assignment, $\mathcal{E}(\mathbf{x}|G) = \mathbf{x}^\top L \mathbf{x}$ is the objective function or *assignment energy* we wish to minimize and:

$$\alpha = \sqrt{\frac{\text{Vol}(A)}{\text{Vol}(V) \text{Vol}(B)}}, \quad \beta = \sqrt{\frac{\text{Vol}(B)}{\text{Vol}(V) \text{Vol}(A)}}. \quad (2)$$

The algorithm in [3], here called the NCut algorithm, solves a relaxation of the minimum NCut problem by dropping the integer constraint in Eq. 1. The new optimization problem can be solved via generalized eigenvector decomposition,

$$L \mathbf{x} = \lambda D \mathbf{x}. \quad (3)$$

The algorithm then selects the eigenvector \mathbf{x} with second-smallest eigenvalue, and partitions V by thresholding \mathbf{x} [3].

2.2. Classical Edge Weight for Image Segmentation

A crucial step in developing efficient segmentation solvers using NCut is to define how the function w is computed. In the original NCut work and in early subsequent work [16, 17, 18], the w combined two grouping cues in a single value:

$$\begin{aligned} w(i, j) = \exp \left(-\frac{\|I(i) - I(j)\|^2}{2\sigma_I^2} - \frac{\|X(i) - X(j)\|^2}{2\sigma_X^2} \right) \\ \times \mathbb{1}(\|X(i) - X(j)\| < r), \end{aligned} \quad (4)$$

where $I(j)$ and $X(j)$ are the appearance (such as the color) of pixel j and its spatial location on image I , respectively, $\mathbb{1}(\cdot)$ is the indicator function, and r , σ_I and σ_X have fixed values.

2.3. Drawbacks of the Traditional Approach

The NCut formulation based on the above weight function presents several drawbacks. For one, it is computationally inefficient to construct the above graph for high resolution images, since it requires visiting each pixel and their neighboring locations within a radius r . Secondly, this graph is potentially dense, which poses memory and runtime difficulties during eigenvector decomposition. NCut using the weight as in Eq. 4 is also known to be inefficient, even for small images [10].

Moreover, calibrating the values for σ_X and σ_I is challenging [14]. Finally, the optimization in Eq. 1 on the graph constructed using Eq. 4 lacks interpretability [14]. The only understanding we can extract from its solution is that it encourages similar pixels to be grouped together, which is commonplace for any spectral clustering algorithm.

3. PROPOSED METHODOLOGY

3.1. New Graph Formulation

Inspired by [4] and [2], we show that a sparse graph formulation efficiently tackles the issues with the classical NCut formulation. Our graph construction starts by considering a grid graph G_{grid} whose vertices correspond to image pixels, with edges of weight $\mu > 0$ between each pair of neighboring pixels. From G_{grid} , we create a new graph G_{all} by adding k extra nodes, each corresponding to one of the k unique colors in I . Each node on G_{grid} is then connected to the extra node corresponding to its color with an edge of unitary weight. This graph formulation is computationally attractive for its sparsity. Assuming $k \ll n$, G_{all} only requires $O(n)$ edges. When segmenting I , we only make use of the assignment vector for the grid nodes.

3.2. Interpretation of the Cut on G_{all}

Let W_{grid} and L_{grid} be the adjacency and Laplacian matrices of G_{grid} , respectively. Let W_{all} and L_{all} be the analogous to G_{all} . These matrices are related to each other as follows:

$$W_{\text{all}} = \begin{bmatrix} W_{\text{grid}} & H \\ H^\top & 0 \end{bmatrix}, \quad L_{\text{all}} = \begin{bmatrix} L_{\text{grid}} + I & -H \\ -H^\top & D_n \end{bmatrix}$$

where $H \in \mathbb{R}^{n \times k}$ is a one-hot encoding of the colors in I , i.e. $H(i, j) = \mathbb{1}\{I(i) = j\}$, and $D_n \in \mathbb{R}^{k \times k}$ is diagonal such that $D_n(j, j) = n_j$, where n_j is the number of pixels in I with color j . Let \mathbf{x} and \mathbf{y} be the assignment vectors for the nodes in G_{grid} and for the extras nodes, respectively. Note that $\mathbf{x} \in \{-\alpha, \beta\}^n$ and $\mathbf{y} \in \{-\alpha, \beta\}^k$, where α and β are computed using Eq. 2 on the graph G_{all} . Let $\mathbf{z} = [\mathbf{x}|\mathbf{y}]$ be \mathbf{x} and \mathbf{y} concatenated. The objective in Eq. 1 then becomes:

$$\begin{aligned} \mathcal{E}(\mathbf{z}|G_{\text{all}}) &= \mathbf{z}^\top L_{\text{all}} \mathbf{z} \\ &= \mathbf{x}^\top (L_{\text{grid}} + I) \mathbf{x} - 2(H\mathbf{y})^\top \mathbf{x} + \mathbf{y}^\top D_n \mathbf{y}. \end{aligned} \quad (5)$$




Noticing that $D_n = H^\top H$, we derive the energy associated with the assignment \mathbf{z} of the nodes on G_{all} :

$$\mathcal{E}(\mathbf{z}|G_{\text{all}}) = \|\mathbf{x} - H\mathbf{y}\|_2^2 + \mathbf{x}^\top L_{\text{grid}} \mathbf{x}. \quad (6)$$

The first term in the above expression accounts for the number of pixels that are assigned to a partition that is not the same as the partition its color is assigned to. In fact, if we define n_{mismatch} as the number of these mismatches, we have:

$$\|\mathbf{x} - H\mathbf{y}\|_2^2 = (\alpha + \beta)^2 n_{\text{mismatch}}. \quad (7)$$

Table 1: Quantitative results on synthetic images in terms of JAC and runtime. The data was generated using four different noise models on three different ground truth patterns. The lower the JAC value, the better.

														
	Noise Type	Noise Level	Prop.	NCut	MixNCut	MGSC	Prop.	NCut	MixNCut	MGSC	Prop.	NCut	MixNCut	MGSC
JAC	Gauss.	$\sigma_g^2 = 0.5$	0.033	0.566	0.035	0.080	0.019	0.642	0.015	0.043	0.020	0.255	0.019	0.027
		$\sigma_g^2 = 1.5$	0.141	0.756	0.172	0.280	0.074	0.696	0.062	0.135	0.092	0.485	0.081	0.192
	S&P	$d = 0.3$	0.036	0.430	0.096	0.097	0.008	0.469	0.041	0.068	0.019	0.212	0.055	0.017
		$d = 0.7$	0.073	0.617	0.314	0.111	0.025	0.670	0.275	0.170	0.048	0.402	0.175	0.050
Average runtime (s)			0.27	13.41	14.30	167.64	0.21	12.92	15.48	147.45	0.19	12.89	13.08	157.81

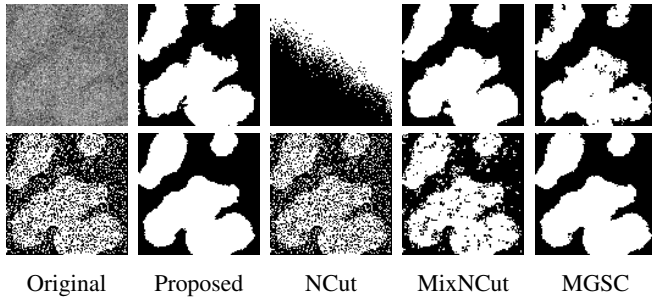


Fig. 1: Qualitative results on synthetic images. Top: Gaussian noise, $\sigma_g^2 = 1.5$. Bottom: Salt & Pepper, $d = 0.7$.

Now, because of the grid nature of G_{grid} , the second term in Eq. 6 accounts for the number of neighboring pixel pairs that are assigned to different segments:

$$\mathbf{x}^\top L_{\text{grid}} \mathbf{x} = \mu(\alpha + \beta)^2 n_{\text{boundary}}, \quad (8)$$

where n_{boundary} stands for the number of pixels on the boundary of the final segmentation. Finally, noticing that $(\alpha + \beta)^2 = \text{Vol}(V) / (\text{Vol}(A) \text{Vol}(B))$ from Eq. 2, we have that:

$$\mathcal{E}(\mathbf{z} | G_{\text{all}}) = \frac{\text{Vol}(V)}{\text{Vol}(A) \text{Vol}(B)} (n_{\text{mismatch}} + \mu n_{\text{boundary}}). \quad (9)$$

Minimizing $\mathcal{E}(\mathbf{z} | G_{\text{all}})$ for \mathbf{x} and \mathbf{y} , results in finding a partition of G_{all} that trades off between spacial coherence (neighboring pixels should belong to the same segment) and color cohesion (pixels in a segment should have colors belonging to the same subset of available intensities) via the value of μ . Minimizing the multiplicative factor in Eq. 9 also encourages a balanced partition of the nodes in G_{all} .

3.3. Improvements

3.3.1. Soft color linkage

Despite the simplicity and computational efficiency of the above result, it does not explicitly use the pixel color intensi-

ties. This means that we would still achieve the same solution to Eq. 1 even if we randomly relabeled the set of available colors. In our experiments, we test the performance of a softer version of the graph described in the previous sections. In this new graph construction, each node i in G_{grid} is linked to all extra nodes with an edge of weight given by

$$w'(i, c) = \exp\left(-\frac{\|I(i) - c\|^2}{2\sigma^2}\right) \quad (10)$$

instead of the unitary weight from the original approach. The interpretation of the solution of Eq. 1 under this new graph is left for future work.

3.3.2. Case when k is large

Our method assumes k , the number of unique colors in I , to be small compared to n . Although this assumption is satisfied for gray scale images, it becomes unrealistic for colored ones. In this case, we vectorize the RGB color space using K -means clustering. The weights in Eq. 10 are then computed using the average RGB color in each cluster. This approach also alleviates the issue posed in the previous section.

4. NUMERICAL EXPERIMENTS

4.1. Experimental Setup

For performance evaluation, we assessed the segmentations via the Jaccard Dissimilarity measure (JAC), defined as:

$$\text{JAC} = 1 - \max(J(R, S), J(R, \neg S)) \quad (11)$$

where R and S are the ground truth image and segmentation, respectively, and $J(R, S) = |R \cap S| / |R \cup S|$ is the Jaccard Index [19]. $\neg S$ is the segmentation with labels swapped.

For our synthetic results, we contaminate three different background and foreground square patterns (intensities of either 0 and 1) of side length ℓ with either additive zero mean

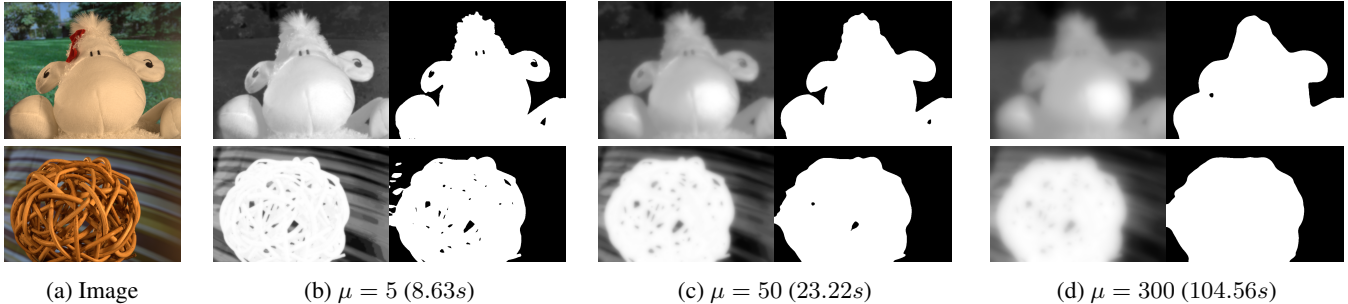


Fig. 2: Qualitative results on RGB images for various μ . (b)-(d) show the eigenvector from Eq. 3 (left) and the corresponding segmentation (right). The image sizes are 800×618 (top) and 800×524 (bottom). Average runtimes are shown in parentheses.

and variance σ_g^2 Gaussian noise or Salt & Pepper with noise density d . The generated images are then rescaled and discretized, so the color intensities are integers in $[0, 255]$. We also test our method using two RGB images from the Alpha Matting dataset [20]. For each of them, we set $k = 256$ in their preprocessing stage (ref. Section 3.3.2).

We compare our proposed method with NCut and two more spectral methods for unsupervised segmentation: Multi Graph Spectral Clustering (MGSC) [21] and MixNCut [14]. For the later two, we create two separate graphs, a grid one for pixel locations and a fully connected one for color data, as described in [14]. When using all these techniques, we refrain from any sparsification algorithm for simplicity. For NCut, we also set $r = \infty$ in Eq. 4 for experimental simplicity and so that we can compare similar graph formulations.

The experiments ran on an Apple M1 Pro Chip (8 core CPU, 14 core GPU) with 16 Gb of RAM memory and were coded in Python 3.9.7 using Numpy 1.21.4 and Scipy 1.7.3¹.

4.2. Results and Discussion

In Table 1, we show the quantitative assessment of our proposed method for images with $\ell = 100$ pixels and two different pairs of noise contaminations for generating each synthetic image under the three proposed ground-truth patterns. For our method, we depict the best JAC when considering the result from trying μ and $\sigma \in [0, 1, \dots, 10]$. For the other methods, we tuned their available parameters and report their best JAC results. In the same table, we also display the average runtime for generating each of the best results' performance in each method per pattern. In Figure 1, we qualitatively compare the best results of each method under two challenging noise levels. These results demonstrate that our method greatly over performs the comparative methods in terms of runtime, a consequence of its sparse nature, while also being competitive in terms of JAC, attaining almost perfect segmentations in most challenging scenarios.

In Figure 2, we qualitatively evaluate the effect of μ to the final segmentation. In these experiments, σ is set to 0. In this

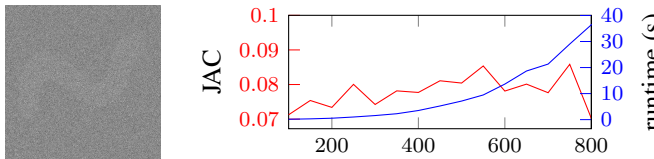


Fig. 3: Segmentation results for varying image sizes. Left: a sample image for $\ell = 500$. Right: the runtime and JAC value results varying ℓ (on the x -axis).

same figure, we also qualitatively demonstrate our method's performance and runtime in large RGB images. Here, we note that μ has the effective role of smoothing the borders of the final segmentation, removing artifacts or boundary details as it increases.

Finally, in Figure 3 we present the average runtime and JAC values for the segmentations of the three patterns of them. We vary the image side lengths ℓ from 100 to 1000 and contaminated each image with zero mean Gaussian noise with $\sigma_g^2 = \ell/100$, which means that images get increasingly hard with size. We again keep $\sigma = 0$ in our proposed algorithm. These results demonstrate that our method scales well despite its spectral nature and generates high quality segmentations on large images even in very challenging noise settings.

5. CONCLUSION AND FUTURE DIRECTIONS

In this paper, we introduce a new spectral algorithm for image segmentation that overcomes some historical issues found in the Normalized Cuts framework and in its related methods. We employ an efficient sparse graph, whose usage under the traditional Normalized Cuts optimization problem leads to an interpretable cut value. We also show that our method is fast and produces high quality results for large RGB imagery and under high synthetic noise settings. For future work, we will derive an interpretation of the cut found on the graph proposed in Section 3.3.1 and extend our methodology to superpixel images—which can further still improve the overall scalability of our proposed method—and multi-region image segmentation.

¹A demo code for this paper is available at www.github.com/rahul-palnitkar/Sparse-Graph-Spectral-Segmentation.

6. REFERENCES

- [1] Richard Szeliski, *Computer vision: algorithms and applications*, Springer Nature, 2022.
- [2] Leo Grady, “Multilabel random walker image segmentation using prior models,” in *2005 IEEE computer society conference on computer vision and pattern recognition (CVPR’05)*. IEEE, 2005, vol. 1, pp. 763–770.
- [3] Jianbo Shi and Jitendra Malik, “Normalized cuts and image segmentation,” *IEEE Transactions on Pattern Analysis and Machine Intelligence*, vol. 22, no. 8, pp. 888–905, 2000.
- [4] Meng Tang, Lena Gorelick, Olga Veksler, and Yuri Boykov, “Grabcut in one cut,” in *Proceedings of the IEEE international conference on computer vision*, 2013, pp. 1769–1776.
- [5] Ashif Sikandar Iquebal and Satish Bukkapatnam, “Consistent estimation of the max-flow problem: Towards unsupervised image segmentation,” *IEEE Transactions on Pattern Analysis and Machine Intelligence*, vol. 44, no. 5, pp. 2346–2357, 2020.
- [6] Jeova FS Rocha Neto, Pedro Felzenszwalb, and Marilyn Vazquez, “Direct estimation of appearance models for segmentation,” *SIAM Journal on Imaging Sciences*, vol. 15, no. 1, pp. 172–191, 2022.
- [7] Shervin Minaee, Yuri Y Boykov, Fatih Porikli, Antonio J Plaza, Nasser Kehtarnavaz, and Demetri Terzopoulos, “Image segmentation using deep learning: A survey,” *IEEE transactions on pattern analysis and machine intelligence*, 2021.
- [8] Ulrike Von Luxburg, “A tutorial on spectral clustering,” *Statistics and computing*, vol. 17, no. 4, pp. 395–416, 2007.
- [9] Charless Fowlkes, Serge Belongie, Fan Chung, and Jitendra Malik, “Spectral grouping using the nystrom method,” *IEEE transactions on pattern analysis and machine intelligence*, vol. 26, no. 2, pp. 214–225, 2004.
- [10] Pablo Arbelaez, Michael Maire, Charless Fowlkes, and Jitendra Malik, “Contour detection and hierarchical image segmentation,” *IEEE transactions on pattern analysis and machine intelligence*, vol. 33, no. 5, pp. 898–916, 2010.
- [11] Xinlei Chen and Deng Cai, “Large scale spectral clustering with landmark-based representation,” in *Twenty-fifth AAAI conference on artificial intelligence*, 2011.
- [12] Lingfei Wu, Pin-Yu Chen, Ian En-Hsu Yen, Fangli Xu, Yinglong Xia, and Charu Aggarwal, “Scalable spectral clustering using random binning features,” in *Proceedings of the 24th ACM SIGKDD International Conference on Knowledge Discovery & Data Mining*, 2018, pp. 2506–2515.
- [13] Li He, Nilanjan Ray, Yisheng Guan, and Hong Zhang, “Fast large-scale spectral clustering via explicit feature mapping,” *IEEE transactions on cybernetics*, vol. 49, no. 3, pp. 1058–1071, 2018.
- [14] Jeova FS Rocha Neto and Pedro F Felzenszwalb, “Spectral image segmentation with global appearance modeling,” *arXiv e-prints*, pp. arXiv–2006, 2020.
- [15] Tijn De Bie and Nello Cristianini, “Fast sdp relaxations of graph cut clustering, transduction, and other combinatorial problems,” *The Journal of Machine Learning Research*, vol. 7, pp. 1409–1436, 2006.
- [16] Lihi Zelnik-Manor and Pietro Perona, “Self-tuning spectral clustering,” *Advances in neural information processing systems*, vol. 17, 2004.
- [17] Wenchao Cai, Jue Wu, and Albert CS Chung, “Shape-based image segmentation using normalized cuts,” in *2006 International Conference on Image Processing*. IEEE, 2006, pp. 1101–1104.
- [18] Wenbing Tao, Hai Jin, and Yimin Zhang, “Color image segmentation based on mean shift and normalized cuts,” *IEEE Transactions on Systems, Man, and Cybernetics, Part B (Cybernetics)*, vol. 37, no. 5, pp. 1382–1389, 2007.
- [19] Paul Jaccard, “Étude comparative de la distribution florale dans une portion des alpes et des jura,” *Bull Soc Vaudoise Sci Nat*, vol. 37, pp. 547–579, 1901.
- [20] Christoph Rhemann, Carsten Rother, Jue Wang, Margrit Gelautz, Pushmeet Kohli, and Pamela Rott, “A perceptually motivated online benchmark for image matting,” in *2009 IEEE conference on computer vision and pattern recognition*. IEEE, 2009, pp. 1826–1833.
- [21] Dengyong Zhou and Christopher JC Burges, “Spectral clustering and transductive learning with multiple views,” in *Proceedings of the 24th international conference on Machine learning*, 2007, pp. 1159–1166.